 doi:10.20944/preprints202107.0170.v1

Article

New evidence of MIS 3 relative sea level changes from the Messina Strait, Calabria (Italy)

Fabrizio Antonioli[1], Lucio Calcagnile[2], Luigi Ferranti[3], Giuseppe Mastronuzzi[4], Carmelo Monaco[5,6,7], Paolo Orrù[9], Gianluca Quarta[3], Fabrizio Pepe[10], Giovanni Scardino[4], Giovanni Scicchitano[4], Paolo Stocchi[11] and Marco Taviani[12,13,14]

1 INGV, Roma, Italy; fabrizioantonioli2@gmail.com (F.A.)
2 CEDAD, Department of Mathematics and Physics "Ennio de Giorgi"University of Salento, and INFN-Lecce, Italy; lucio.Calcagnile@unisalento.it (L.C.); gianluca.quarta@unisalento.it (G.Q.)
3 Dipartimento di Scienze della Terra, dell'Ambiente e delle Risorse, Napoli University, Italy; luigi.ferranti@unina.it (L.F.)
4 Dipartimento di Scienze della Terra e Geoambientali, Università degli Studi di Bari Aldo Moro, 70125 Bari, Italy; giuseppe.mastronuzzi@uniba.it (G.M.); giovanni.scardino@uniba.it (G.Sc.); giovanni.scicchitano@uniba.it (G.S.)
5 Dipartimento di Scienze Biologiche Geologiche e Ambientali, Catania University, Italy; cmonaco@unict.it (C.M.)
6 CRUST-Interuniversity Center for 3D Seismotectonics with Territorial Applications, 66100 Chieti Scalo, Italy
7 Istituto Nazionale di Geofisica e Vulcanologia, Osservatorio Etneo, 95131 Catania, Italy
9 Dipartimento di Scienze Chimiche e Geologiche, Cagliari University; orrup@unica.it (P.O.)
10 Dipartimento di Scienze della Terra e del Mare, Palermo University; fabrizio.pepe@unipa.it (F.P.)
11 NIOZ Royal Netherlands Institute for Sea Research, Coastal Systems Department, and Utrecht University, The Nederland; paolo.stocchi@nioz.nl (P.S.)
12 Institute of Marine Sciences (CNR-ISMAR) Bologna, Italy 40129 Bologna, Italy; marco.taviani@cnr.it (M.T.)
13 Stazione Zoologica Anton Dohrn, 80122 Napoli, Italy
14 Biology Department, Woods Hole Oceanographic Institution, Woods Hole, MA 02543-1050 U.S.A

Abstract: Investigation of sea-level positions during the highly-dynamic Marine Isotope Stage 3 (MIS 3: 29-61 kyrs BP) proves difficult because: i) in stable and subsiding areas, coeval coastal sediments are currently submerged at depths of few to several tens of meters below present sea level; ii) in uplifting areas, the preservation of geomorphic features and sedimentary records is limited due to the erosion occurred during the Last Glacial Maximum (LGM) with sea level at depth of -130 m, followed by marine transgression that determined the development of ravinement surfaces.

This study discusses previous research in the Mediterranean and elsewhere, and describes new fossiliferous marine deposits laying on metamorphic bedrock of Cannitello (Calabria, Italy). Radiocarbon ages of marine shells (about 43 kyrs cal BP) indicate that these deposits, presently between 28 and 30 meters above sea level, formed during MIS 3.1. Elevation correction of the Cannitello outcrops (considered in an intermediate-to-far-field position with respect to the ice sheet) with the local vertical tectonic rate and Glacial Isostatic Adjustment (GIA) rate allows to propose a revision of the eustatic depth for this highstand. Our results are consistent with recently proposed estimates based on a novel ice sheet modelling technique.

Keywords: Marine Isotope Stage 3, sea level, tectonics, GIA, Calabria

1. Introduction

1.1. MIS 3 sea level historical background

Marine Isotope Stage 3 was a time of strong climatic contrasts, likely in response to changes in the Atlantic Meridional Overturning Circulation [1]. A precise assessment of

sea level positions for this interstadial proves to be elusive and controversial (lastly revised by Siddall et al., [2]). For instance, estimates of global sea-level during MIS 3 range between -15 and -87 m [3–7]. One major problem relies upon reconstructions based upon indirect proxies, like the widely used stable oxygen stratigraphy that translates into ice volumes (and, therefore, related sea-level ups and downs) the geochemical signals incorporated into benthonic or planktonic foraminifera from core records [3,8]. However, one primary advantage to investigate sea-level positions based upon cores is the continuity of such records. This contrasts the discontinuous record offered by Pleistocene coral reefs and uplifted or buried sedimentary sequences, which have, on the other way, the advantage to provide direct physical evidence of former sea levels [2,9]. The highly diverse and variegated nature of available markers, coupled with intrinsic difficulties to precisely date deposits >40 kyr, accounts in recognising MIS 3 as 'enigmatic' [2]. From a climatic perspective, MIS 3 is a crucial time interval since it was characterised by frequent (millennial) and abrupt thermal oscillations, strongly reverberating on variations of sea levels [2,10,11].

It is, therefore, of paramount importance to estimate the sea level position during this interstadial. Most reconstructions on MIS 3 seem to exclude that sea level ever reached depths greater than – 60/-50 m [2,6,9].

Aim of this paper was to discuss MIS 3 marine deposits in Calabria (Italy, Figure 1), a strongly uplifting area of the central Mediterranean. We selected the Cannitello site in southern Calabria where uplift rates have been calculated using a flight of raised Pleistocene terraces, that include last interglacial terraces [12].

1.2. Regional setting

Calabria is the emerging part of a forearc terrane belonging to the Ionian subduction system. The subducting Ionian lithosphere dips ~ 70–80° northwestward down to a depth of 450–500 km (see inset in Figure 1; [13–16]). The upper plate of the subduction system, from west to east, consists of back-arc basins that become younger southeastwards (Vavilov and Marsili basins; [17–19]), an arc-shaped volcanic ridge (i.e., Aeolian islands), and a forearc-accretionary wedge system including the Calabrian Arc (CA) [20,21].

The CA experienced vigorous uplift during the Quaternary [22,23]. Vertical movements cumulate the effects of both regional and local processes. The latter was related to footwall uplift along extensional faults [24–29]. Hanging-wall subsidence counteracts the effects of regional uplift, which in the long-term prevails [28,30].

The CA has been stretched by WNW-ESE oriented Quaternary extension [30–32]. Today belts of active extensional faults run along the chain axis and the Tyrrhenian side of the northern and southern C A, respectively.

 doi:10.20944/preprints202107.0170.v1

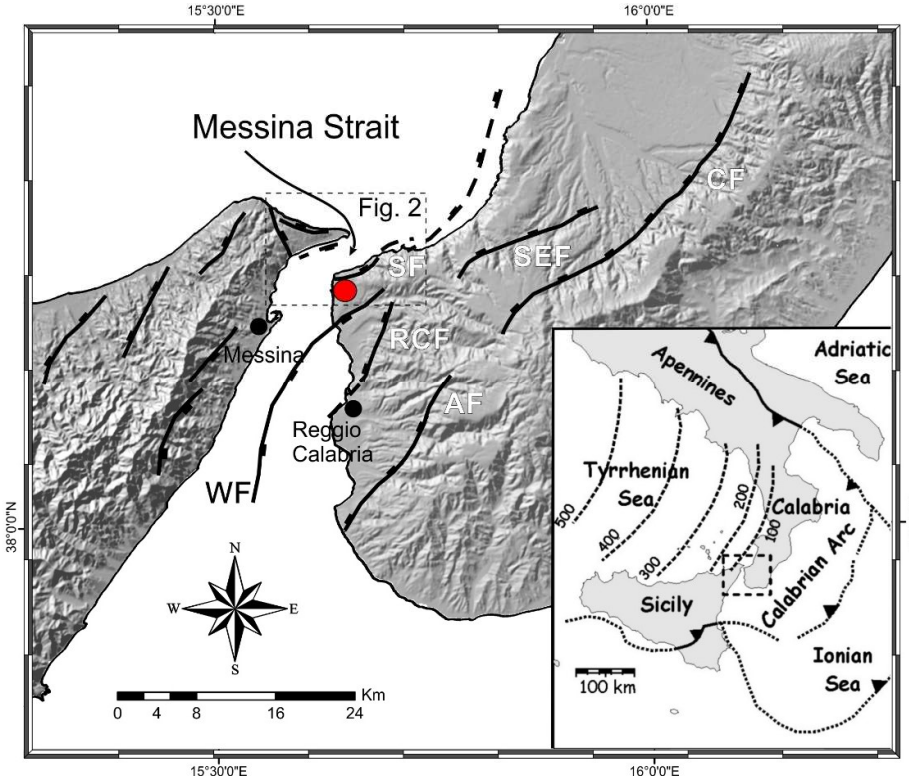

Figure 1. Tectonic setting of the Messina Strait region in the southern part of the Calabrian Arc. Active faults (thick solid lines barbed on the downthrown side) after Monaco and Tortorici [33] and Barreca et al. [34]: AF, Armo Fault; RCF, Reggio Calabria Fault; CF, Cittanova Fault; SEF, S. Eufemia Fault; SF, Scilla Fault, W-Fault. The red balloon indicates the studied Cannitello site. Inset shows the location of the study area in the tectonic setting of the Central Mediterranean (from Chiarabba et al. [35]).

1.3. Study area

The study area is located on the Calabrian side of the Strait of Messina (southern sector of the Calabrian Arc, Figure 1). The Strait is a Pliocene-Quaternary basin limited by ENE-WSW to NNE-SSW striking normal faults offsetting Palaeozoic metamorphic basement rocks and Miocene terrigenous covers [24,25,36,37](Figure 1). The stratigraphic architecture of the basin consists of Lower Pliocene chalks, Upper Pliocene-Lower Pleistocene calcarenites, up to the middle Pleistocene deltaic Gravels and Sands Fm [38–40]. These sequences are unconformably overlain by Pleistocene alluvial and terraced coastal deposits [12,23,41–43], ranging in elevation from 40 to 1200 m a.s.l. The marine terraced series is partly displaced by the Scilla Fault and by the Cappuccini Fault, which bound the Piale High [24,25,30,44–46] to the north and south, respectively (Figure 2). The terraced deposits consist of fossiliferous calcarenites or sublittoral sands and sandy gravels, more or less cemented, directly lying on the Palaeozoic metamorphic basement or on the Pliocene-Pleistocene deposits [23,41,43]. The marine deposits generally pass upwards to continental alluvial and/or colluvial reddish silt with sands and gravels levels.

The lowest and youngest terrace extends along the coast, from Villa S. Giovanni to Cannitello area, where it seals the western end of the Scilla Fault, with an inner edge at 45 m a.s.l. Balescu et al. [47] correlate this terrace with the Oxigen Isotope Stage 3 (60 ka, [48]) based on the Thermo Luminescence and Optically Stimulated Luminescence (OSL) ages of associated aeolian sands. This paleoshoreline corresponds to the lowest one mapped by Monaco et al. [12](Figure 1) and attributed by the authors to the MIS 3.3.

The upper terraces extend around the Piale High, extensively outcropping on the hanging wall of the Scilla Fault northward and along the south-west side with inner edges at elevations between 60-85 and 205 m a.s.l. The complete sequence outcrops only on the Piale High (Figure 2), where the oldest terraces show inner edges at elevations between 285 and 520 m a.s.l. These terraces are represented by wave-cut platforms directly resting on the crystalline substratum and covered by silts and reddish continental sands.

The absolute dating obtained by Balescu et al. [47], crossed with geomorphological correlations to deposits containing *Thetystrombus latus* (Gmelin, 1791*) (= Persististrombus latus* (Gmelin, 1791) = *Strombus bubonius* Lamarck, 1822*)* in the Reggio Calabria area [23,42,49,50], robustly constrain the age of the whole sequence, whose highest terrace has been attributed to the MIS 11 (405 kyrs, Figure 2). A more elevated terrace, associated with marine deposits containing *Globorotalia truncatulinoides excelsa* [51], reaches an altitude of 680 m. It was attributed to the MIS 25 (~950 ka) by Miyauchi et al. [23], but more probably must be referred to the MIS 19 (~730 ka). A complete map of coastal-alluvial Quaternary terraces, obtained from Miyauchi et al. [23], is shown in Figure 2 where, following the authors, the highest terraces are assigned to middle-lower Pleistocene.

Preprints (www.preprints.org) | NOT PEER-REVIEWED | Posted: 7 July 2021 doi:10.20944/preprints202107.0170.v1

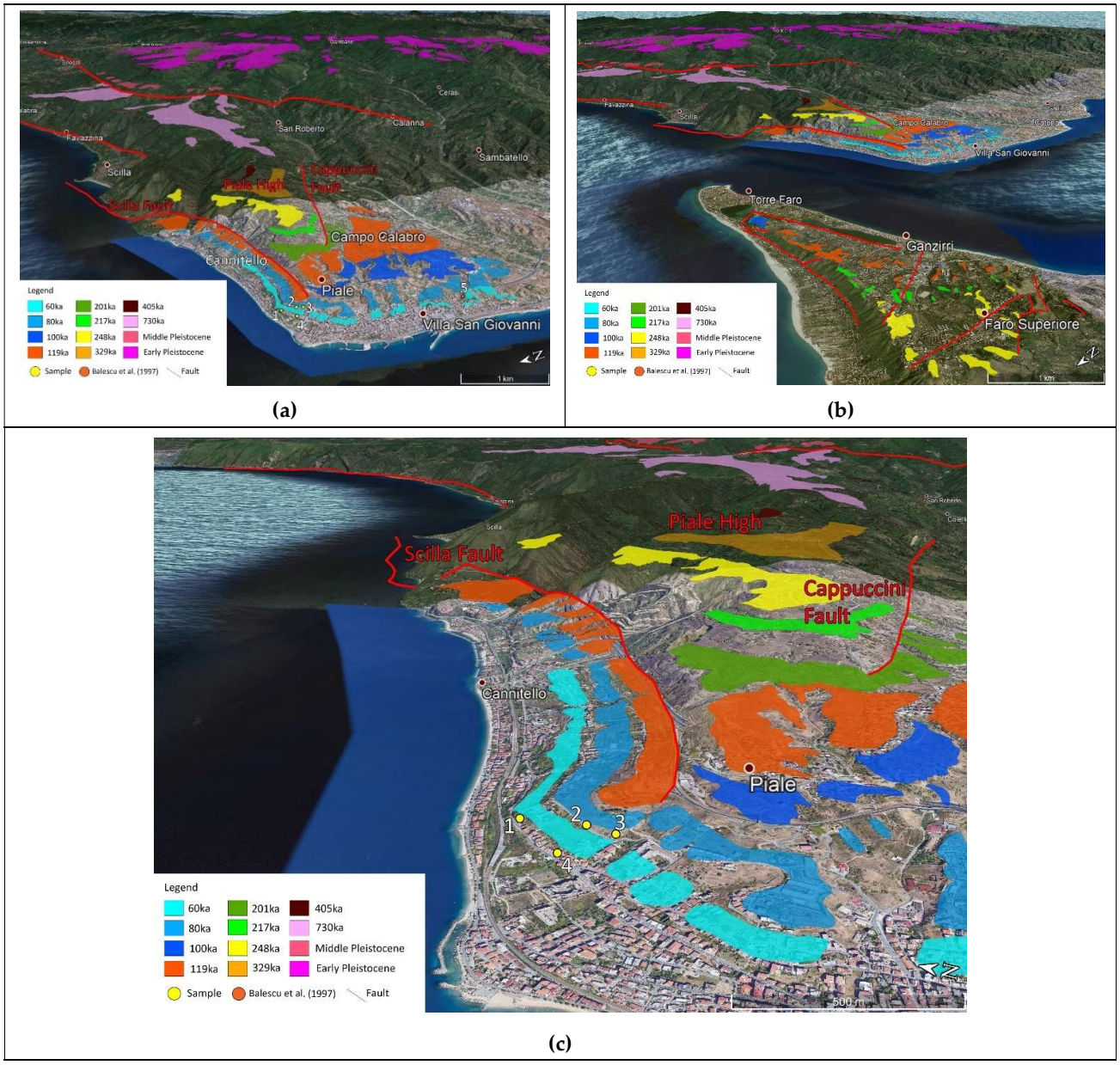

Figure 2. (a), (b), (c) Maps of the terraced sequence (see Figure 1 for location).

2. Previous studies on MIS 3

2.1 MIS3 in the global context

On a global scale, a limited number of studies have specifically considered MIS 3 RSL records [52]. For istance, deposits and paleoshorelines ascribed to MIS 3 have been found in Grand Bahamas where Richards et al. [53] found evidence that the MIS 3.3 highstand exceeded the depth of -18.1 m as speleothem GB-89-25-5C shows a hiatus between 63.7 and 58.5 kyrs. However, the highstand does not exceed the -15 meters depth of flowstone DWBAH [54,55] (Figure 3). The Bahamas flowstome DWBAH may prove to represent a sealevel marker of utmost global importance, since encompassing a continuous record

Preprints (www.preprints.org) | NOT PEER-REVIEWED | Posted: 7 July 2021 doi:10.20944/preprints202107.0170.v1

from 326 up to 37 kyrs BP, with 5 hiatuses corresponding to many marine highstands. The comparsion of DWBAH altitude data with the speleothem of Richards et al. [53], not presenting hiatus for MIS 3 (-18.1 m), sets an upper limit (-16 m) for the MIS 3.3 highstand.

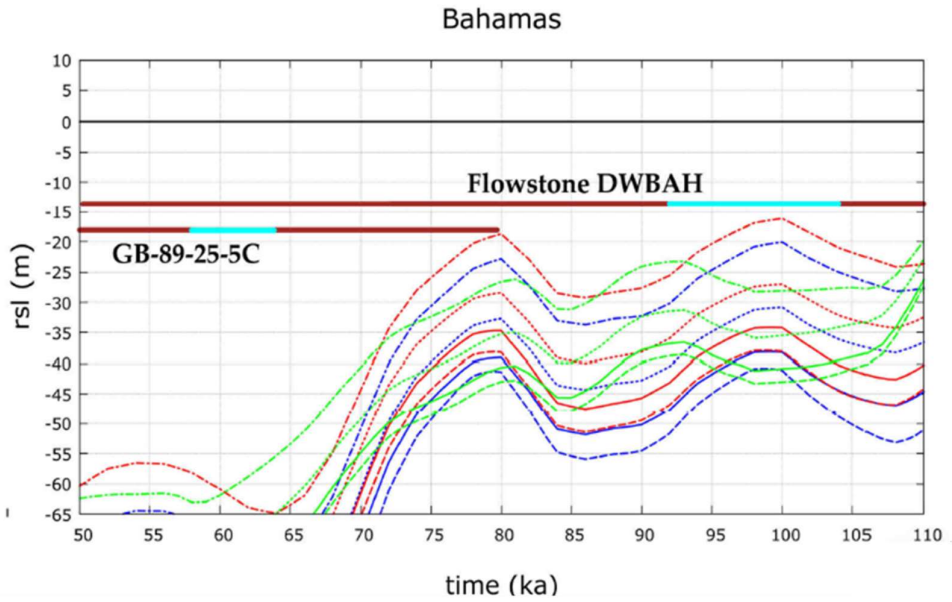

Figure 3. Constraints on MIS 3 depth from the Bahamas. The submerged speleothem GB-(89) sampled in the Blue Hole (Bahamas) at -18.1 m [53] shows a hiatus between 63.7 and 58.5 kyrs. Glacial and hydro-isostatic Adjustments (GIA) at Bahamas is similar to that of the Central Mediterranean sea [56]. Predicted RSL curves for the ICE-5G (red curves), ICE-6G (green curves), and ANICE-SELEN (blue curves) ice sheet models in combination with MVP 1–3 mantle viscosity profiles (solid, dashed and dotted lines, respectively) at each site and with respect to the measured elevations.

Lambeck et al. [8] described MIS 3 deposit at about -50m/-60m along the coasts of Bonaparte Gulf and Huon Peninsula. However, such results could be affected by an underestimation of tectonics contribute. An integrated study of the Gulf of Mexico offshore using high-resolution seismics, extensive coring and dating (^{14}C AMS ages and stable isotope stratigraphy) supplies considerable evidence of a remarkable MIS3 sea level high-stand. The shoreline (as a brackish lagoon proxy) probably reached up to -15/-18 m below the present sea level at ^{14}C ages of about 37-40 ky BP [4]. Evidence of circum-Antarctic emerged marine deposits attributed to MIS 3 is summarised by Berkman et al. [57]. Wide shelfal sectors in the Weddell and Ross seas were probably under open-water conditions at this time [58,59].

Pico et al. [60] refined estimates of global ice volume during MIS 3 by employing sediment cores in the Bohai and Yellow Sea, that record migration of the paleo-shoreline at ~50-37 ka through a transition from marine to brackish conditions, defining a peak global mean sea level of 38 ± 7 m during the interval 50-37 ka.

2.2 A Mediterranean MIS3 perspective

In the Mediterranean region, information with sea-level implications for the MIS 3 mainly relates to offshore cores (e.g., [61–64]) and offshore and onland boreholes [65–73]. These data chiefly report the position of continental or marine deposits ascribed to MIS 3 within marginal sequences, but their value to assess with confidence the sea level positions is rather limited. Additional reference to MIS 3 is found in other records, like submerged terraces [74] or prehistoric contexts [75].

Regarding the eastern Mediterranean, Dogan et al. [76] focused their attention on fossilferous units cropping along the Samandag coast, Turkey. They applied the electron spin resonance (ESR) method to molluscs identifyig MIS 5.1 and MIS 3 deposits. The study estimated for the area a fast uplift probably related to the vertical component of the strike-slip active faults in the Samandage Antakya Fault Zone. Data analysis and vertical tectonic movements lead us to think of an eustatic altitude of MIS 3 in this coastal area of Turkey of -40 meters.

Kirci-Elmas et al. [64], based upon floro-faunal arguments, propose that Izmit Gulf was connected with the Black Sea and the Mediterranean Sea at the beginning of MIS-3 (ca. 52.0 - 40.0 ky BP).

A borehole drilled by 'Regione Emilia-Romagna' in the Po Plain (Italy) onshore the Adriatic coast encountered, at about 30 m below the surface, sandy layers interpreted as representing a fluviatile facies [65]. Noticeably, fresh shells of the marine intertidal gastropod *Nassarius circumcinctus* (A. Adams, 1852) picked from these sands were ^{14}C dated at ca. 37 kyr (A. Viesce, pers. com.). Thus, the sandy layer might represent a former marine shoreline, currently located about 30 m below the surface and ascribable to MIS 3 [75]. This evidence merits further investigation because it may shed new light on sea level variations during MIS 3.

On the other side of the north Adriatic Sea, in Lošinj (Croatia), Brunović et al. [77] attributed a deposit found at about -50 m, in a brackish-to freshwater lacustrine body, to MIS 3. Antonioli et al. [56], in a review paper on the use of submerged speleothems in the Mediterranean Sea, provided helpful information about sea level during MIS 3 for several areas of the Mediterranean basin. Along the Croatian side of the northern Adriatic Sea, speleothems collected inside submerged caves proved that MIS 3 never exceeded the a -18.8 m depth (after correction for subsidence affecting the coastal area [78]).

Along the Tyrrhenian sea coastline, submerged stalagmites collected in the Argentarola Island showed an uninterrupted continental deposition during MIS 3, testifying sea level did not reach values higher than about -21.7m [79,80].

Along the Ionian coast of south-eastern Sicily, Dutton et al. [81] analysed several stalagmites found inside caves developed along paleo shorelines presently submerged at about -20m and -40m [82]. Samples collected along the deepest paleo shorelines show a continuous growth of continental layers inside the speleothems during MIS 3, proving that sea level has never been shallower than -38m (using a tectonic rate of 0.2 mm/yrs).

Along the Ionian Sea coast of northern Calabria, a flight of eleven terraces dated to the Middle-Late Pleistocene indicates an uplift at ~1 mm/yrs [83–85]. The lowermost

 doi:10.20944/preprints202107.0170.v1

terrace (T1), with an inner edge at an elevation between 11-24 and ~17 m at the foot of the Pollino and Sila mountain ranges, respectively, was attributed to MIS 3.1 by Ferranti et al. [83] based on a ^{14}C calibrated age of 44±0.4 ka from a '*Cardium*' shell at the Pollino range coast. The sample was taken from a conglomerate deposit in the bank of a stream cutting terrace T1, but, although resedimented in the recent alluvial system, it ostensibly comes from terrace T1, and thus the existence of MIS 3 was ascertained. Based on borehole data, Santoro et al. [84] document a ~10-15 m thickness of coarse marine deposits for T1 and suggested that the terrace is polycyclic and includes both MIS 3.3 and 3.1, as it was sea-flooded during two peaks of the MIS 3. Santoro et al. [84,85] indicate at the Pollino coast the existence of a lower terrace T0 with an inner edge at 5-11 (average ~8) m, suggesting that T1 (average ~15 m) is related to MIS 3.3. This attribution would support that the age from the '*Cardium*' shell refers to terrace T0 that is thus attributed to MIS 3.1. With an uplift rate of 0.9 mm/yr established by Santoro et al. [85] on the MIS 5.5 terrace (dated by Ferranti et al. [83]), a 43 ka old terrace with an inner margin presently at +8 m should have been uplifted of 38 m; thus it formed at -30 m below present sea-level.

Further north, raised marine deposits that have been attributed to MIS 3 by means of OSL age determinations have been recognized along the Ionian coast of Basilicata [86,87].

3. The Cannitello site

3.1 Geological-paleontological description

Several outcrops of fossiliferous sublittoral deposits area are found in the Cannitello location. The sites have been positioned through GPS RTK, orthometric heights have been obtained using the IGM (Italian Geographic Military Institute) grids for the Calabria area.

Table 1. Cannitello studied sites altitude, see also Figure 2

Site number	Latitude	Longitude	GPS Altitude m	Google Earth Altitude m
CANNITELLO 1	38,232280 N	15,644851 E	28,382	30
CANNITELLO 2	38,230440 N	15,644630 E	57,201	57
CANNITELLO 3	38,229399 N	15,643769 E	48,122	47
CANNITELLO 4	38,230805 N	15,642728 E	27,282	28

The most relevant site (Cannitello 1, elevation 28 m; Figure 2, Table 1) is stratigraphically located beneath the outer margin of the terrace attributed to MIS 3.3 [12]. The 3 m thick stratigraphic section (Figure 4a) presents fine sands at the base , with flat parallel lamination in a marly silty matrix with fine gravel levels (1). This deposit is engraved by a surface of sub-planar erosion on medium sands in silty matrix in plane-parallel position (2) characterised at the base by a level of heterometric pebbles (2a) with a thickness of 10 cm. A Mitylus shell (Sample 1, Table 2) was sampled from one of the levels above to fragments of bivalves and gastropods (2b position of Figure 4a).

In the top part of this level, the plane-parallel lamination resumes and levels of lamellibrancs fragments are observed. Medium sands with inclined lamination follow upward above an erosion surface proximal submerged beach environment foreset (3).

Preprints (www.preprints.org) | NOT PEER-REVIEWED | Posted: 7 July 2021 doi:10.20944/preprints202107.0170.v1

The section is sealed at the top by continental deposits represented by a colluvial level (4) and a stratified slope deposit with poorly elaborated subangular pebbles (5).

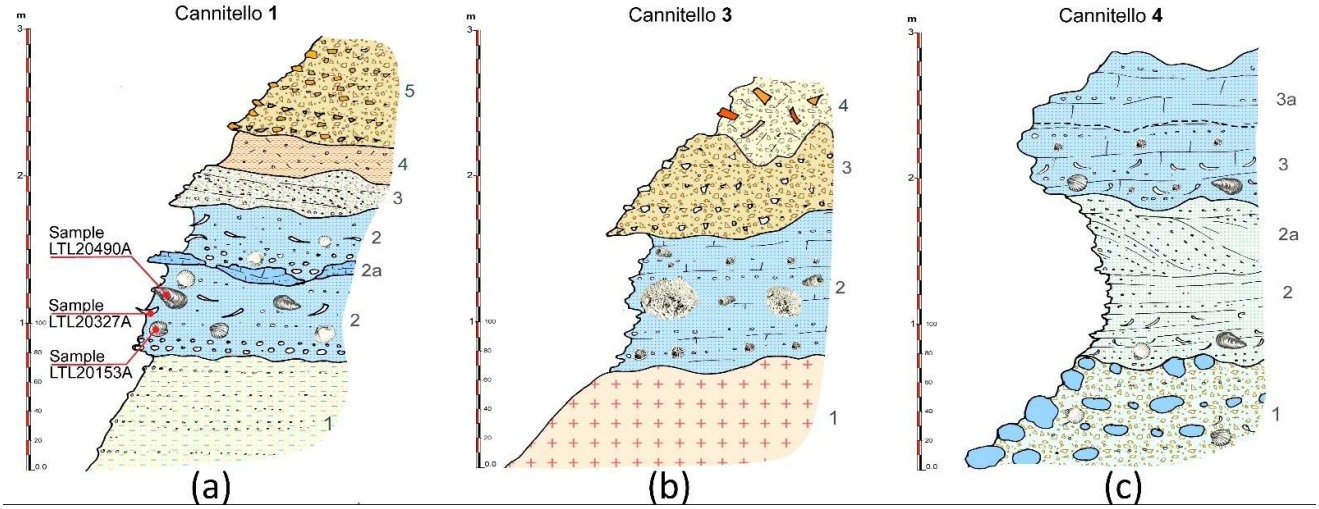

Figures 4 (a), (b), (c). Stratigraphic sections of the sites Cannitello 1, 3, 4. For Cannitello 1 we have highlighted the position of the sampled and dated fossils of Table 2.

The basal sedimentary level (2) of the Cannitello 3 site rests upon an irregular erosion surface carved within the altered metamorphic bedrock (1). Marine sediments likely documenting mesolittoral and infralittoral environment are represented by fine sands and gravels with flat parallel lamination. This level is characterized by a weakly-cemented a skeletal bryzoan hash dominated by *Miriapora truncata* (Pallas, 1766) biosomes. These marine deposits are overlaid by continenta scree deposits congtaning aligned sub-angular pebbles (3), in turn blanketed by anthropic fill materials (4).

The site Cannitello 4 exposes a densely-packed shelly rudstone with abundant but degradeded biosomes and bioclasts pertaining to infra-mesolittoral organisms, such as bivalves, e.g. *Arca cf noe* Linnaeus, 1758, cf. *Acanthocardia tuberculata* (Linnaeus, 1758), gastropods as *Jujubinus cf striatus* (Linnaeus, 1758), *Alvania* sp., naticid, *Tritia* sp, and scaphopods (*Antalis* sp.). Finally, a level of broken Mytilus shells was found. Although a precise bathymetric assessment based upon fossils is problematic, nontheless an estimated paleodepth between 10-30 m is not unreasonable (Figures 2, 4, 6).

In addition to these sites attributable to MIS3 (see below), we identified other older Pleistocene marine deposits which could generated some confusion in the field. For example, the site named Cannitello 2 (57.2 m elevation), located above the terrace attributed to MIS 3.3 [12], consists of a well-cemented calcarenite encasing among other deep-water scleractinian corals, i.e. *Desmophyllum dianthus* (Esper, 1794), *D. pertusum* (Linnaeus, 1758) and *Caryophyllia* sp. In all likeness, this facies represents a Late to Middle Pleistocene bathyal deposit plastering a former submarine cliff, a common case in this region submitted to important uplift [88].

Preprints (www.preprints.org) | NOT PEER-REVIEWED | Posted: 7 July 2021 doi:10.20944/preprints202107.0170.v1

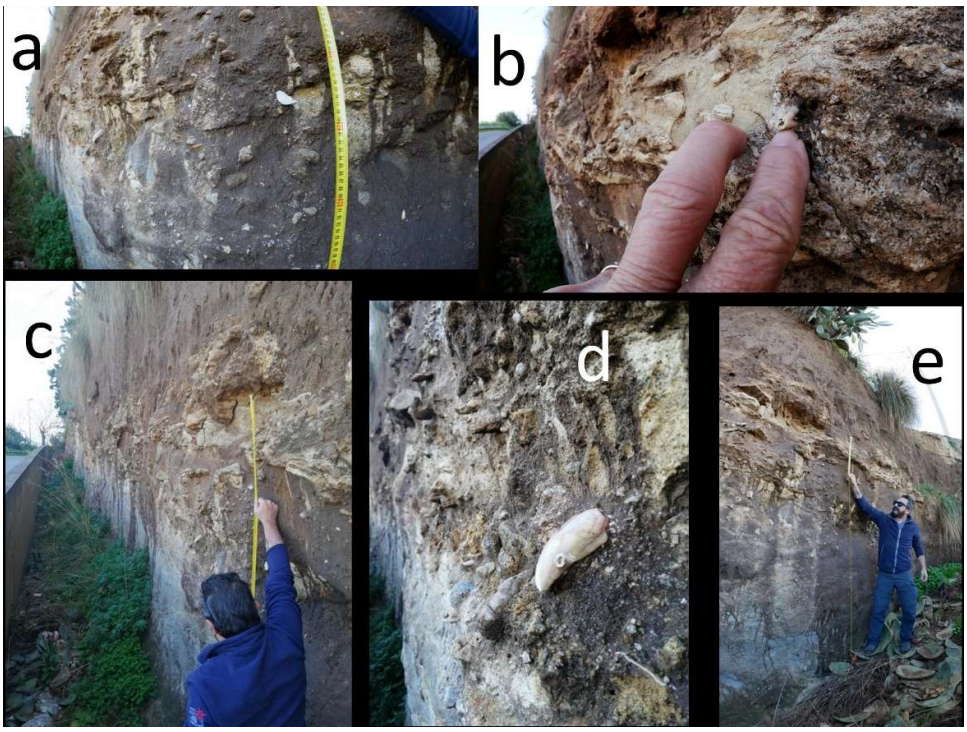

Figure 5. The Cannitello 1 outcrop. a,b,c,e) Size and some details of the section. d) the radiocarbon aged (sample LTL20153A of Table 2) *Mytilus* in situ.

Figure 6 The Cannitello 4 outcrop. a,b,c,d) Size, and some details of the section.

 doi:10.20944/preprints202107.0170.v1

3.2 Sampling and radiocarbon analyses

Dated samples come from silt-sandy deposits at Cannitello 1 site, and were easily extracted from the poorly cemented matrix. Radiocarbon dating analyses were carried out at CEDAD-Centre for Applied Physics, Dating and Diagnostics, Department of Mathematics and Physics, University of Salento in Lecce-Italy [89]. The samples were first analysed at the optical microscope in order to highlight possible macro-contamination such as adhering residues of soils. They were then etched with H_2O_2 to remove the external layer and then rinsed with demonised water. The purified sample was then hydrolysed under vacuum by using H_3PO_4, the released CO_2 was then cryogenically purified and then converted to graphite by using H_2 as a reducing agent at 600°C on Fe powder acting as a catalyst. For all three samples, ~1mg of graphite was obtained which is considered optimal for the following isotopic analyses. The obtained graphite was then used to measure the $^{14}C/^{12}C$ and $^{13}C/^{12}C$ isotopic ratio at the AMS (Accelerator Mass Spectrometry) beamline at CEDAD based on a 3 MV Tandetron (Mod. HVEE 4130HC) accelerator. The radiocarbon age of the samples was then calculated from the measured $^{14}C/^{12}C$ ratios by applying the radiocarbon decays law and after correcting the measured terms for mass fractionation and processing blanks. In particular C1 carbonate standards (Carrara Marble completely depleted in ^{14}C supplied by IAEA (International Atomic Energy Agency) were used to estimate the machine and chemical processing blank during the whole process. Conventional radiocarbon ages were then calibrated in calendar years by using the last released calibration dataset for marine organisms (MARINE20) [90] and using a local marine reservoir correction term ΔR=-88±50 yrs as obtained by Siani et al. [91] and recalculated for the MARINE20 curve (Table 2).

Table 2 Radiocarbon ages: samples at Cannitello 1 site see also Figures 5,6,7

Sample	Radiocarbon age years (BP)	Age years Cal BP 1sigma	$\delta^{13}C$ (‰)(	Fossil	Altitude Satellite m
LTL20153A	>48000	-	2.5 ± 0.2	*Mytilus*	28.3±0.2
LTL20327A	40887 ± 320	43152± 304	+4.2 ± 0.4	Gastropod	28.3±0.2
LTL20490A	40828 ± 300	43092± 273	0.3 ± 0.2	*Arca noae*	29.3±0.2

Table 2 lists the radiocarbon dating results. Two samples fall within MIS 3.1, and one resulted out of the radiocarbon range (>48,000 years).

4 GIA modelling

4.1 Model setting

Existing estimations of MIS 3.1 and MIS3.3 RSL depths carry the contribution of both vertical land and mean sea surface (geoid) variations in response to the ice sheets

 doi:10.20944/preprints202107.0170.v1

fluctuations. Indeed, surface mass transfer from the oceans to the continents, and viceversa, besides altering the global oceans mass and volume (eustatic sea-level change), do trigger solid Earth deformations and gravitational and rotational perturbations that affect the geoid. This process is known as glacial- and hydro-isostatic adjustment (GIA) and causes local RSL changes to deviate from the global mean (eustatic) as a function of the distance from the ice sheets. Here we account for the GIA process by solving the gravitationally self-consistent sea level equation (SLE) [53-54] and using the open-source program SELEN [55-57]. Accordingly, we compute the local RSL curves for prescribed solid Earth rheological models and ice sheets models.

We assume a self-gravitating, rotating, spherically symmetric, radially stratified, deformable but not compressible Earth model. The latter is 1-dimensional, implying that all the relevant rheological parameters are afunction of the Earth's radius only. The outer shell of the model is perfectly elastic and represents the lithosphere. Between the lithosphere and the inviscid core is the mantle, characterised by linear Maxwell viscoelastic rheology.

We employ a four-layer mantle discretisation where the upper mantle (UM), the lower upper mantle (LUM), the transition zone (TZ) and the lower mantle (LM) are characterised by uniform viscosity according to the VM2 profile (see Table 3). We combine this vertical stratification with a lithosphere thickness of 90 km and use it as a reference model. Furthermore, we consider three mantle viscosity profiles (MVPs) that are characterised by an increase in the vertical viscosity gradient from MVP1 to MVP3 (see Table 4). We use these three profiles in combination with a 100 km thick Lithosphere.

Table 3

VM2	LT (km)	UM (x 10^{21} Pa·s)	LUM (x 10^{21} Pa·s)	TZ (x 10^{21} Pa·s)	LM (x 10^{21} Pa·s)
	90	0.67	0.44	0.46	2.53

Table 4

MVPs	LT (km)	UM (x 10^{21} Pa·s)	TZ (x 10^{21} Pa·s)	LM (x 10^{21} Pa·s)
MVP1	100	1	1	2
MVP2	100	0.5	0.5	5
MVP3	100	0.25	0.5	10

We employ four ice sheets models chronologies that can be divided into two cathegories:

1 Delta-18O-dependent ice sheets models:

1.1 ICE-5G and ICE-6G [92–95]: these global models describe the ice-sheet thickness variations over North America, Eurasia, Greenland and Antarctica for the last 123 ka. The ice thickness chronology between 26 ka and present-day is constrained by geological and modern geodetical observations through an iterative procedure that involves the solution of the SLE for an a priori ice sheets configuration and a prescribed fixed solid Earth model (mantle viscosity profile and Lithosphere thickness). The ice sheets

volumetric evolution between 123 and 26 ka is tuned to the delta-18O curve [94] and, where possible, constrained by geological evidences that define the ice sheets coverage and margins.

1.2 ANICE-SELEN [96,97]: this global chronology model is the result of an inverse forward modelling procedure where the delta-18O stack [94] is decoupled into global ice sheets volume and deep-water temperature. For this purpose, 3D thermomechanical ice-sheet models for North America, Eurasia, Greenland and Antarctica, are dynamically coupled to SELEN in order to include all the GIA feedbacks. ANICE-SELEN is not constrained by geological or instrumental data.

2. Delta-18O-independent ice sheets models:

2.1 PaleoMIST 1.0 [98]: this model stems from the combination of simplified 2-Dimensional ice flow modelling and geological data that constrain the ice-sheets boundaries in space and time (2,500 years temporal snapshots). The reconstructed ice sheets margins, once combined with the topography, allow for the calculation of the basal sheat stress that, for a prescribed ice flow law, yields the 2-Dimensional, steady state ice thickness variations within the ice sheets margins. The model is then improved by an iterative procedure where the SLE is solved to account for realistic changes in topography. RSl curves are computed for each iterative step and compared to dated near-field RSL observations (RSL database). The itereative process is run until convergence is found. Accordingly, the ice sheet model is independent of the far-field and global sea-level proxies that are based on deep sea delta-18O records. We employ two versions of PaleoMIST 1.0: (i) Minimal MIS 3 and (ii) Maximal MIS 3, respectively with and without major retreat of the Laurentide Ice Sheet.

Therefore, the eustatic sea-level curves of ICE-5G, ICE-6G and ANICE-SELEN, which reflect the ice-sheets volume variation in time and expressed in meters of equivalent sea level, strongly depend on the benthic oxygen curve. The eustatic curve of PaleoMIST 1.0, instead, depends on the areal extent of the ice sheets, which is constrained by surface geological indicators, and is completely independent of the benthic oxygen curve.

We employ the reference VM2 profile (Table 3) combined with all the four ice sheets models, while the three MVPs (Table 4) are only used for ICE-5G, ICE-6G and ANICE-SELEN.

4.2 Numerical GIA predictions

Numerical RSL predictions for the three ice sheets models that depend on the delta-18O record are very close to the corresponding eustatic curves, which represent the ice sheets volume variation in time expressed as meters of equivalent sea level (Figure 7). The expected GIA variability, i.e. the vertical difference of the GIA-modulated RSL curves with respect to the eustatic, is ~2.5 m for ICE-5G (red curves in Figure 7) and ICE-6G (blue curves in Figure 7) and ~ 5.0-10.0 m for the ANICE-SELEN model runs (green curves in Figure 7). This confirms previous findings of Antonioli et al. [56,99] and stresses the major role of glacio-eustasy in this area and during the MIS 3 period.

Preprints (www.preprints.org) | NOT PEER-REVIEWED | Posted: 7 July 2021 doi:10.20944/preprints202107.0170.v1

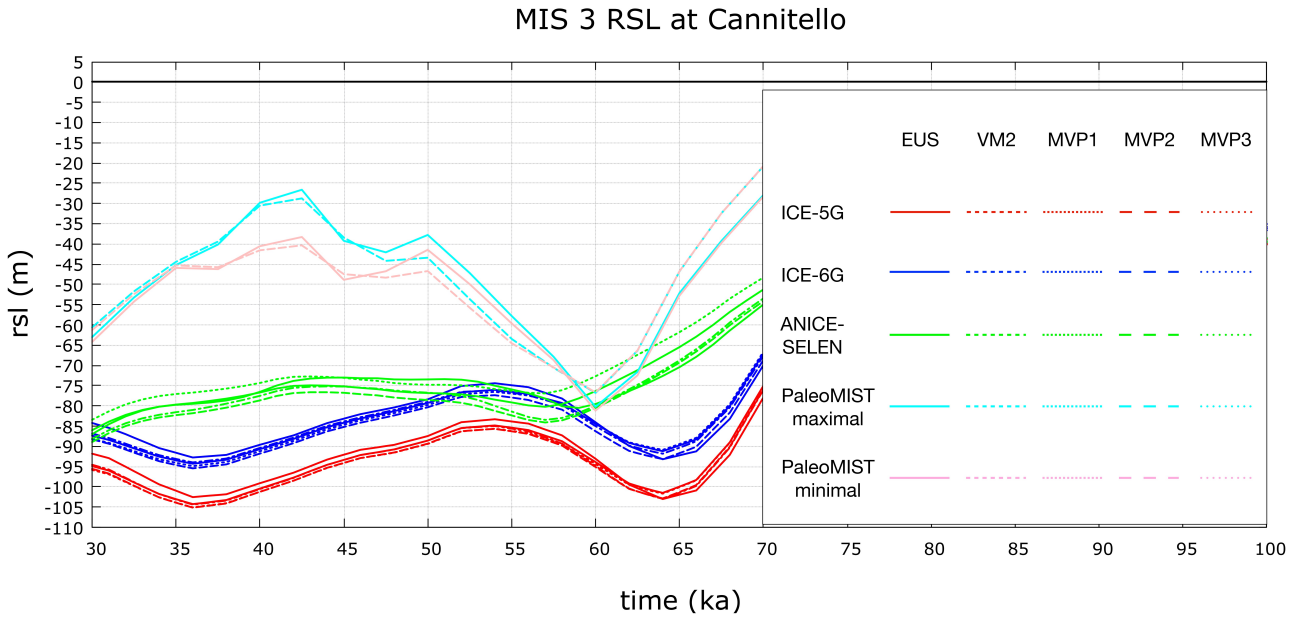

Figure 7 Predicted RSL curves for four ice sheets models: ICE-5G (red), ICE-6G (blue), ANICE-SELEN (cyan), and PaleoMIST 1.0 maximal and minimal (cyan and pink, respectively). The solid curves represent the eustatic. The dashed and dashed-dotted curves represent the GIA-modulated RSl predictions.

Data-models comparison reveals that the predicted MIS 3.1 and MIS 3.3 RSL elevations for ICE-5G, ICE-6G and ANICE-SELEN are significantly lower than the observed values (corrected for tectonics). The GIA variability cannot explain the differences of 35-60 m and 30-50 m, respectively, at the MIS 3.1 and 3.3.

The predicted RSL curves for PaleoMIST 1.0 Maximal and Minimal MIS 3 (cyan and pink curves in Figure 7), both in combination with VM2 mantle profile (Table 3), are significantly above the ICE-5G, ICE-6G and ANICE-SELEN curves (Figure 7). This implies that the PaleoMIST 1.0 ice sheets model is characterised by smaller ice volumes during the time frame under consideration.

Interestingly, the PaleoMISt 1.0 curves converge towards a minimum at 60 ka which is in line with the other models. Accordingly, the predicted RSL elevation at the MIS 3.3 is ~30 m lower than the observed. However, After 60 ka, the predictions for PaleoMIST 1.0 diverge and maximum highstands of -30 m and -40 m is obtained at 42.5 ka for, respectively, the Minimal and Maximal MIS 3 versions. These values are in agreement with the observed MIS 3.1 elevation.

5. Discussion

Published global information coupled with new field data from southern Calabria suggest that the quantity of melted ice during MIS 3 could have been underestimated in the global curves [5,6]. In general, observed sea-level markers are largely consistent showing a sea level between -18 and -40 meters, with 30-40 meters difference with respect

to the global curves. To note, an agreement exists between predicted sea-level and observed markers with Gowan et al. [98] for MIS 5.3, 5.1 and 3.1.

The radiocarbon ages (Table 1) of samples collected at 28 m, allow to attribute Cannitello 1 at MIS 3.1; they are consistent with the age of the overlying marine terraces (see Table 5, Figure), in particular with the MIS 3.3 terrace at 45 metres (64 kyrs, [47]).

The sedimentary features of the studied deposits suggest they formed at the foot of a cliff in a high environmental energy (slope almost overlooking the sea with a relief that reaches 5-600 m). Today the sea-bottom rapidly deepens respectively to -50 and - 100 m at 120 and 230 m offshore. For these reasons, it is quite difficult to determine with great precision the depth of the foot of the paleocliff on which fossils sampled and aged at Cannitello 1 accumulated. The bivalves and gastropods are sourced from infralittoral to circalittoral environments, with some mixing. Important clues come from the observation that: (ì) pebbles within the deposit are covered by algal encrustations, (ìì) there is not evidence of tractive sedimentary structures. Together, those considerations seem to indicate an environment at the transition between infralittoral and circalittoral zones, below the wave closure depth (estimated at ca. -10-20 m below the coeval sea level).

In order to frame the aged fossil beach in the whole sequence of terraces, in Table 5 we considered: a) the elevation of inner margin or fossil beaches of the whole flight in this sector of southern Calabria, b) the age of terraces or fossils deposit, and c) the eustatic sea level. Based on these data, it is possible to note that the uplift rates are rather constant. We calculated the uplift rates of the distinct terraces by adding the observed elevation to the coeval eustatic position and dividing it by the age of the deposit or terrace.

The inner edges of the overlying terraces have been mapped with an estimated error in elevation of ±5 m [12,23], depending on phenomena of erosion and/or deposition of alluvial sediments following the emergence of the terraces. Consequently, the elevations above sea level of the paleo-shorelines reported in Table 5 must be considered as mean values. This uncertainty is however negligible in estimating the long-term Quaternary uplift rates involving time spans of tens to hundreds of thousands of years.

Table 5. 1) Elevation of sea level markers, from: this paper [1]; Monaco et al. [12] [2]; Miyauchi et al. [23] [3]. The distinct inner edges have been mapped by these authors with an error margin in the elevation of ±5 m, depending on erosion and depositional processes following the emergence of the terraces. An error of ± 10 m has been applied for the fossils raised deposit*. This implies that the elevations above sea level of the inner edges must be considered as mean values. **2**) Marine Isotopic Stage attribution based on dating and geomorphological correlations (see text for explanations). **3**) Age from: this paper [1]; Balescu et al. [47] [2]; Miyauchi et al. [23] and Monaco et al. [98] [3]; Antonioli et al.[100] [4] and Senegalese fauna; Dutton et al. [80] [5]. Lisieki and Raymo [94] [6] **4**) Eustatic sea level from: Gowan et al. [98] and this paper [1]; Waelbroek et al. [6] [2]; Dutton et al. [80] [3]; Lisieki and Raymo [94] [4]. **5)** Uplift rate calculated for each stage and **6)** as average value for the middle-late Pleistocene.

1 Observed elevation of terraces inner margins or fossils/infra/circalittoral raised deposits* m	2 Marine Isotopic Stage (MIS)	3 Age (ka)	4 Eustatic sea level (m)	5 Uplift rate mm\yrs	6 Mean uplift rate mm\yrs
*28[1]	3.1	43.1[1]	-34[1]	1.2 -1.4	
45[2]	3.3	64 [2]	-48[2]	1.4	
85[2]	5.1	81[3]	-16[3]	1.2	**1,3**
120[2]	5.3	101[3]	-19[4]	1.4	
165[2]	5.5	119[4]	+8.35[4]	1.3	
205[2]	7.1	201,5[5]	-16[4]	1.3	
285[2]	7.3	217,2[5]	-17,5[4]	1.1	
345[2]	7.5	248.9[5]	-13[4]	1,2	
415[2]	9	329[6]	+4[4]	1.3	
520[3]	11	405[6]	+5[4]	1.2	
680[3]	19	760[6]	-5[4]	0.9	**0,9**

The whole flight of terraces of southern Calabria (partly directly aged, and partly intercorrelated on stratigraphic arguments) gives us a fairly robust estimation of the uplift rates of the entire coastal area, where the lower values have been calculated for the Middle-Lower Pleistocene (older than 730 ka, 0.9 mm/yrs), and the higher ones, between 1.2 and 1.4 mm/yrs, have been estimated for the Middle-Late Pleistocene. It should also be noted that uplift rates have undergone an acceleration in the Holocene (last 3-4 ka Cal BP), reaching values of 1.8-2 mm/yrs along the coastline, at the footwall of the Scilla Fault [83].

The uplift rate estimated for Middle-Late Pleistocene terraces supports our reconstruction of the eustatic elevation of the MIS 3.1 deposits. For this estimation, we used the sea level curve of Gowan et al. [98] (Figure 7) where the average between PaleoMIST 1.0 maximal (-40 m) and minimal (-29 m) of the curve at 43 kyrs is -34.5 m. As mentioned before, a rigorous paleobathymetric assessment of the units under scrutiny proves

problematic due to the lack of unquestionable sea level markers. Therefore, we choose a conservative approach not adopting a bathymetric correction for Cannitello 1 but an error of ± 10 m. The resulting uplift rate ranges between 1.2 and 1.4 mm/yrs, in agreement with estimation from older terraces.

Uplift rate results are also consistent with our reconstruction of MIS 3.3 eustatic sea level elevation. Indeed, they confirm that the the value proposed by Monaco et al. (2017) at -48 meters, based on the estimation of Waelbroeck et al. [102], may be valid.

Our numerical results and observational data confirm that the MIS 3 RSL changes at Cannitello are governed by glacio-eustasy, whereas GIA plays a secondary role. While the $\delta^{18}O$ dependent ice sheets models result in RSl curves that are always significantly lower than the observations, PaleoMIST 1.0 is the only model capable of returning a MIS 3.1 elevation that is in agreement with the observations. Indeed, we observe that there is a discrepancy (of at least 30-40 meters) between the eustatic altitude of the MIS 3 of all global curves and that suggested by the observed points. Therefore, we support the contention that a reduction of global ice sheets volumes across the MIS 3, and specifically at the MIS 3.1 and 3.3, is needed. Our results confirm previous evaluations by Pico et al. [101] and Gowan et al. [98].

Conclusions

Marine fossiliferous deposits representing former infra-circa littoral environments have been identified in the Messina Strait sector of southern Calabria, a region typified by important neotectonic uplift. Field evidence, appraised uplift rates of the more ancient terraces, and 14C age of fossil deposits sampled at altitudes of 28 m, strongly suggest that such deposits formed during MIS 3.1.

Given the overall scantiness of MIS3 marine outcrops, only explorable in coastal areas subject to important uplift, we consider the southern Calabrian site relevant for the assessment of past sea levels during this still little-known interstadial.

The GIA results suggest that the $\delta^{18}O$ -based ice-sheets models appear to overestimate significantly the ice-sheets volumes during the MIS 3.1 and 3.3. Our data are in agreement with Gowan et al. [98], raising by 40 metres the eustatic contribution to sea level during interstadials MIS 3.1, 5.1, 5.3 with respect to current global sea level curve scenarios. Further, our reconstruction well agrees with records proposing MIS 3 sea levels at depths between -18 and -40 m.

Acknowledgments: This study has been partly funded by the project MUSE 4D-Overtime tectonic, dynamic and rheologic control on destructive multiple seismic events—Special Italian Faults and Earthquakes: From real 4-D cases to models, in the frame of PRIN 2017. This is Ismar-CNR, Bologna scientific contribution n. 2056

Author Contributions: Conceptualization, F.A., L.F., G.M., C.M. P.O., F.P., G.S., P.S., and M.T.; methodology, P.S., L.C., G.Q.; software, P.S., G.Sc.; formal analysis, L.C., G.Q, P.S.; investigation, F.A., P.O., G.S. F.P. writing—original draft preparation, F.A. C.M., P.O., M.T. F.P.; writing—review and editing, F.A., M.T., C.M. P.O., G.Q., F.P. All authors have read and agreed to the published version of the manuscript

Funding: This research received no external funding

Conflicts of Interest: The authors declare no conflict of interest

Abbreviation	Acronyms
1. MIS	Marine Isotope Stage
2. CA	Calabrian Arc
3. MS	Mediterranean Sea
4. MSL	Mean Sea Level
5. AMS	Accelerator Mass Spectrometry
6. GIA	Glacial and hydro Isostatic Adjustment
7. RSL	Relative Sea Level
8. SLE	Sea Level Equation
9. UM	Upper Mantle
10. LUM	Lower Upper Mantle
11. TZ	Transition Zone
12. LM	Lower Mantle
13. BP	Before Present
14. DWBAH	is the the acronym of a submerged flowstone

References

1. Jonkers, L.; Brummer, G.-J.A.; Peeters, F.J.C.; van Aken, H.M.; de Jong, M.F. Shell Flux and Oxygen Isotope Data of North Atlantic Foraminifera. *Supplement to: Jonkers, L et al. (2010): Seasonal stratification, shell flux, and oxygen isotope dynamics of left-coiling N. pachyderma and T. quinqueloba in the western subpolar North Atlantic. Paleoceanography, 25, PA2204, https://doi.org/10.1029/2009PA001849* 2010.
2. Siddall, M.; Rohling, E.J.; Thompson, W.G.; Waelbroeck, C. Marine Isotope Stage 3 Sea Level Fluctuations: Data Synthesis and New Outlook. *Reviews of Geophysics* **2008**, *46*, doi:https://doi.org/10.1029/2007RG000226.
3. Imbrie, J.; Hays, J.; Martinson, D.; McIntyre, A.; Mix, A.; Morley, J.; Pisias, N.; Prell, W.; Shackleton, N. The Orbital Theory of Pleistocene Climate: Support from a Revised Chronology of the Marine Delta 18O Record. **1984**.
4. Rodriguez, A.; Anderson, J.; Banfield, L.; Taviani, M.; Abdulah, K.; Snow, J. Identification of a −15 m Wisconsin Shoreline on the Texas Inner Continental Shelf. *Palaeogeography, Palaeoclimatology, Palaeoecology* **2000**, *158*, 25–43, doi:10.1016/S0031-0182(00)00027-4.
5. Waelbroeck, C.; Labeyrie, L.; Michel, E.; Duplessy, J.C.; McManus, J.F.; Lambeck, K.; Balbon, E.; Labracherie, M. Sea-Level and Deep Water Temperature Changes Derived from Benthic Foraminifera Isotopic Records. *Quaternary Science Reviews* **2002**, *21*, 295–305, doi:10.1016/S0277-3791(01)00101-9.
6. Siddall, M.; Rohling, E.J.; Almogi-Labin, A.; Hemleben, C.; Meischner, D.; Schmelzer, I.; Smeed, D.A. Sea-Level Fluctuations during the Last Glacial Cycle. *Nature* **2003**, *423*, 853–858, doi:10.1038/nature01690.
7. Antonioli, F. Sea Level Change in Italy until 400 Ka: Comparing Global Sea Level Curves with Observed Data. *Alpine and Mediterranean Quaternary* **2011**, *24*, 11–13.

8. Lambeck, K.; Yokoyama, Y.; Purcell, T. Into and out of the Last Glacial Maximum: Sea-Level Change during Oxygen Isotope Stages 3 and 2. *Quaternary Science Reviews* **2002**, *21*, 343–360, doi:10.1016/S0277-3791(01)00071-3.
9. Chappell, J. Sea Level Changes Forced Ice Breakouts in the Last Glacial Cycle: New Results from Coral Terraces. *Quaternary Science Reviews* **2002**, *21*, 1229–1240, doi:10.1016/S0277-3791(01)00141-X.
10. Voelker, A.H.L. Global Distribution of Centennial-Scale Records for Marine Isotope Stage (MIS) 3: A Database. *Quaternary Science Reviews* **2002**, *21*, 1185–1212, doi:10.1016/S0277-3791(01)00139-1.
11. Kjellström, E.; Brandefelt, J.; Näslund, J.-O.; SMITH, B.; Strandberg, G.; Voelker, A.; Wohlfarth, B. Simulated Climate Conditions in Europe during the Marine Isotope Stage 3 Stadial. *Boreas* **2010**, *39*, 436–456, doi:10.1111/j.1502-3885.2010.00143.x.
12. Monaco, C.; Barreca, G.; Stefano, A.D. Quaternary Marine Terraces and Fault Activity in the Northern Mainland Sectors of the Messina Strait (Southern Italy). *IJG* **2017**, *136 (2017) f.3*, doi:10.3301/IJG.2016.10.
13. Wortel, M.J.R.; Spakman, W. Subduction and Slab Detachment in the Mediterranean-Carpathian Region. *Science* **2000**, *290*, 1910–1917, doi:10.1126/science.290.5498.1910.
14. Piromallo, C.; Morelli, A. P Wave Tomography of the Mantle under the Alpine-Mediterranean Area. *Journal of Geophysical Research: Solid Earth* **2003**, *108*, doi:10.1029/2002JB001757.
15. Chiarabba, C.; De Gori, P.; Speranza, F. The Southern Tyrrhenian Subduction Zone: Deep Geometry, Magmatism and Plio-Pleistocene Evolution. *Earth and Planetary Science Letters* **2008**, *268*, 408–423, doi:10.1016/j.epsl.2008.01.036.
16. Scarfi, L.; Graziella, B.; Barreca, G.; Cannavò, F.; Koulakov, I.; Patanè, D. Slab Narrowing in the Central Mediterranean: The Calabro-Ionian Subduction Zone as Imaged by High Resolution Seismic Tomography. *Scientific Reports* **2018**, *8*, doi:10.1038/s41598-018-23543-8.
17. Carminati, E.; Doglioni, C. Europe: Mediterranean Tectonics. In *Encyclopedia of Geology*; 2004; pp. 135–146.
18. Faccenna, C.; Funiciello, F.; Civetta, L.; D'Antonio, M.; Moroni, M.; Piromallo, C. Slab Disruption, Mantle Circulation, and the Opening of the Tyrrhenian Basins. **2007**, doi:10.1130/2007.2418(08).
19. Faccenna, C.; Molin, P.; Orecchio, B.; Olivetti, V.; Bellier, O.; Funiciello, F.; Minelli, L.; Piromallo, C.; Billi, A. Topography of the Calabria Subduction Zone (Southern Italy): Clues for the Origin of Mt. Etna. *Tectonics* **2011**, *30*, doi:https://doi.org/10.1029/2010TC002694.
20. Corradino, C.; Ganci, G.; Cappello, A.; Bilotta, G.; Calvari, S.; Del Negro, C. Recognizing Eruptions of Mount Etna through Machine Learning Using Multiperspective Infrared Images. *Remote Sensing* **2020**, *12*, 970, doi:10.3390/rs12060970.
21. Pepe, F.; Kanari, M.; Burrato, P.; Corradino, M.; Duarte, H.; Ferranti, L.; Monaco, C.; Sacchi, M.; Tibor, G. *Active Deformation Evidence in the Offshore of Western Calabria (Southern Tyrrhenian Sea) from Ultra-Resolution Multichannel Seismic Reflection Data: Results from the Gulf of Sant'Eufemia*; Copernicus Meetings, 2020;
22. Westaway, R. Quaternary Uplift of Southern Italy. *Journal of Geophysical Research: Solid Earth* **1993**, *98*, 21741–21772, doi:https://doi.org/10.1029/93JB01566.
23. Miyauchi, T.; Dai Pra, G.; Sylos Labini, S. Geochronology of Pleistocene Marine Terrace and Regional Tectonics in the Tyrrhenian Coast of South Calabria, Italy. *Il Quaternario* **1994**, *7*, 17–34.
24. Ferranti, L.; Monaco, C.; Antonioli, F.; Maschio, L.; Kershaw, S.; Verrubbi, V. The Contribution of Regional Uplift and Coseismic Slip to the Vertical Crustal Motion in the Messina Straits, Southern Italy: Evidence from Raised Late Holocene Shorelines. *Journal of Geophysical Research: Solid Earth* **2007**, *112*, doi:https://doi.org/10.1029/2006JB004473.

25. Ferranti, L.; Monaco, C.; Morelli, D.; Antonioli, F.; Maschio, L. Holocene Activity of the Scilla Fault, Southern Calabria: Insights from Coastal Morphological and Structural Investigations. *Tectonophysics* **2008**, *453*, 74–93, doi:10.1016/j.tecto.2007.05.006.
26. Ferranti, L.; Antonioli, F.; Anzidei, M.; Monaco, C.; Stocchi, P. The Timescale and Spatial Extent of Vertical Tectonic Motions in Italy: Insights from Relative Sea-Level Changes Studies. *Journal of the Virtual Explorer* **2010**, *36*, doi:10.3809/jvirtex.2009.00255.
27. Ferranti, L.; Antonioli, F.; Monaco, C.; Scicchitano, G.; Spampinato, C.R. Uplifted Late Holocene Shorelines along the Coasts of the Calabrian Arc: Geodynamic and Seismotectonic Implications. *IJG* **2017**, *136 (2017) f.3*, doi:10.3301/IJG.2017.13.
28. Roberts, G.; Meschis, M.; Houghton, S.; Underwood, C.; Briant, R. The Implications of Revised Quaternary Palaeoshoreline Chronologies for the Rates of Active Extension and Uplift in the Upper Plate of Subduction Zones. *Quaternary Science Reviews* **2013**, *78*, 169–187, doi:10.1016/j.quascirev.2013.08.006.
29. Pepe, F.; Bertotti, G.; Ferranti, L.; Sacchi, M.; Collura, A.; Passaro, S.; Sulli, A. Pattern and Rate of Post-20 Ka Vertical Tectonic Motion around the Capo Vaticano Promontory (W Calabria, Italy) Based on Offshore Geomorphological Indicators. *Quaternary International* **2014**, *332*, 85–98, doi:10.1016/j.quaint.2013.11.012.
30. Jacques, E.; Monaco, C.; Tapponnier, P.; Tortorici, L.; Winter, T. Faulting and Earthquake Triggering during the 1783 Calabria Seismic Sequence. *Geophysical Journal International* **2001**, *147*, 499–516, doi:10.1046/j.0956-540x.2001.01518.x.
31. D'Agostino, N.; Selvaggi, G. Crustal Motion along the Eurasia-Nubia Plate Boundary in the Calabrian Arc and Sicily and Active Extension in the Messina Straits from GPS Measurements. *Journal of Geophysical Research: Solid Earth* **2004**, *109*, doi:https://doi.org/10.1029/2004JB002998.
32. Palano, M.; Ferranti, L.; Monaco, C.; Mattia, M.; Aloisi, M.; Bruno, V.; Cannavò, F.; Siligato, G. GPS Velocity and Strain Fields in Sicily and Southern Calabria, Italy: Updated Geodetic Constraints on Tectonic Block Interaction in the Central Mediterranean. *Journal of Geophysical Research: Solid Earth* **2012**, *117*, doi:https://doi.org/10.1029/2012JB009254.
33. Monaco, C.; Tortorici, L. Active Faulting in the Calabrian Arc and Eastern Sicily. *Journal of Geodynamics* **2000**, *29*, 407–424, doi:10.1016/S0264-3707(99)00052-6.
34. Barreca, G.; Gross, F.; Scarfì, L.; Aloisi, M.; Monaco, C.; Krastel, S. The Strait of Messina: Seismotectonics and the Source of the 1908 Earthquake. *Earth-Science Reviews* **2021**, *218*, 103685, doi:10.1016/j.earscirev.2021.103685.
35. Chiarabba, C.; Jovane, L.; DiStefano, R. A New View of Italian Seismicity Using 20 Years of Instrumental Recordings. *Tectonophysics* **2005**, *395*, 251–268, doi:10.1016/j.tecto.2004.09.013.
36. Tortorici, L.; Monaco, C.; Tansi, C.; Cocina, O. Recent and Active Tectonics in the Calabrian Arc (Southern Italy). *Tectonophysics* **1995**, *243*, 37–55, doi:10.1016/0040-1951(94)00190-K.
37. Aloisi, M.; Bruno, V.; Cannavò, F.; Ferranti, L.; Mattia, M.; Monaco, C.; Palano, M. Are the Source Models of the M 7.1 1908 Messina Straits Earthquake Reliable? Insights from a Novel Inversion and a Sensitivity Analysis of Levelling Data. *Geophysical Journal International* **2013**, *192*, 1025–1041, doi:10.1093/gji/ggs062.
38. Lombardo, G. Studio Stratigrafico Del Plio-Pleistocene Del Bacino Di Reggio Calabria. *Atti Acc. Gioenia di Sc. Nat., Catania* **1980**, *12*, 233–298.
39. Barrier, P. Evolution Paléogéographique Du Détroit de Messine Au Pliocéne et Au Pléistocène. *Giornale di Geologia* **1996**, *3*, 7–24.
40. Monaco, C.; Tortorici, L.; Nicolich, R.; Cernobori, L.; Costa, M. From Collisional to Rifted Basins: An Example from the Southern Calabrian Arc (Italy). *Tectonophysics* **1996**, *266*, 233–249, doi:10.1016/S0040-1951(96)00192-8.

41. Dumas, B.; Gueremy, P.; Lhenaf, R.; Raffy, J. Reliéf et Néotectonique de La Facade Orientale Du Détroit de Messine (Calabre, Italie). *Travaux de la RCP* **1978**, 95–124.
42. Dumas, B.; Gueremy, P.; Lhenaf, R.; Raffy, J. Rates of Uplift as Shown by Raised Quaternary Shorelines in Southern Calabria (Italy). *Zeitschrift fur Geomorphologie* **1987**, *63*, 119–132.
43. Ghisetti, F. Upper Pliocene- Pleistocene Uplift Rates as Indicators of Neotectonic Pattern: An Example from Southern Calabria (Italy). *Zeitschrift fur Geomorphologie, Supplementband* **1981**, *40*, 93–118.
44. Ghisetti, F. L'evoluzione Strutturale Del Bacino Plio-Pleistocenico Di Reggio Calabria Nel Quadro Geodinamico Dell'Arco Calabro. *Bollettino Geologico Italiano* **1981**, *100*, 433–466.
45. Ghisetti, F. Fault Parameters in the Messina Strait (Southern Italy) and Relations with the Seismogenic Source. *Tectonophysics* **1992**, *210*, 117–133, doi:10.1016/0040-1951(92)90131-O.
46. Pirrotta, C.; Barbano, M.; Monaco, C. Evidence of Active Tectonics in Southern Calabria (Italy) by Geomorphic Analysis: The Examples of the Catona and Petrace Rivers. *Italian Journal of Geosciences* **2016**, *135*, 1–45, doi:10.3301/IJG.2015.20.
47. Balescu, S.; Dumas, B.; Guérémy, P.; Lamothe, M.; Lhénaff, R.; Raffy, J. Thermoluminescence Dating Tests of Pleistocene Sediments from Uplifted Marine Shorelines along the Southwest Coastline of the Calabrian Peninsula (Southern Italy). *Palaeogeography, Palaeoclimatology, Palaeoecology* **1997**, *130*, 25–41, doi:10.1016/S0031-0182(96)00119-8.
48. Chappell, J.; Shackleton, N.J. Oxygen Isotopes and Sea Level. *Nature* **1986**, *324*, 137–140, doi:10.1038/324137a0.
49. Bonfiglio, L. Il Tirreniano Di Bovetto e Ravagnese Presso Reggio Calabria. *Quaternaria* **1972**, *16*, 137–148.
50. Dumas, B.; Raffy, J. Late Pleistocene Tectonic Activity Deduced from Uplifted Marine Terraces in Calabria, Facing the Strait of Messina. *Quaternaria Nova* **2004**, *8*, 79–99.
51. Ruggieri, G.; Sprovieri, R. La Definizione Dello Strtotipo Del Piano Siciliano e Le Sue Conseguenze. *Il Naturalista Siciliano* **1975**, *IV*, 187–214.
52. Benjamin, J.; Rovere, A.; Fontana, A.; Furlani, S.; Vacchi, M.; Inglis, R.H.; Galili, E.; Antonioli, F.; Sivan, D.; Miko, S.; et al. Late Quaternary Sea-Level Changes and Early Human Societies in the Central and Eastern Mediterranean Basin: An Interdisciplinary Review. *Quaternary International* **2017**, *449*, 29–57, doi:10.1016/j.quaint.2017.06.025.
53. Richards, D.A.; Smart, P.L.; Lawrence Edwards, R. Maximum Sea Levels for the Last Glacial Period from U-Series Ages of Submerged Speleothems. *Nature* **1994**, *367*, 357–360, doi:10.1038/367357a0.
54. Li, W.-X.; Lundberg, J.; Dickin, A.P.; Ford, D.C.; Schwarcz, H.P.; McNutt, R.; Williams, D. High-Precision Mass-Spectrometric Uranium-Series Dating of Cave Deposits and Implications for Palaeoclimate Studies. *Nature* **1989**, *339*, 534–536, doi:10.1038/339534a0.
55. Lundberg, J.; Ford, D.C. Late Pleistocene Sea Level Change in the Bahamas from Mass Spectrometric U-Series Dating of Submerged Speleothem. *Quaternary Science Reviews* **1994**, *13*, 1–14, doi:10.1016/0277-3791(94)90121-X.
56. Antonioli, F.; Furlani, S.; Montagna, P.; Stocchi, P. The Use of Submerged Speleothems for Sea Level Studies in the Mediterranean Sea: A New Perspective Using Glacial Isostatic Adjustment (GIA). *Geosciences* **2021**, *11*, 77, doi:10.3390/geosciences11020077.
57. Berkman, P.A.; Andrews, J.T.; Björck, S.; Colhoun, E.A.; Emslie, S.D.; Goodwin, I.D.; Hall, B.L.; Hart, C.P.; Hirakawa, K.; Igarashi, A.; et al. Circum-Antarctic Coastal Environmental Shifts during the Late Quaternary Reflected by Emerged Marine Deposits. *Antarctic Science* **1998**, *10*, 345–362, doi:10.1017/S0954102098000406.
58. Taviani, M.; Anderson, J. Response of Biogenic Carbonate Factories to Ice Sheet and Ice Shelf Dynamics: A Largely Deglaciated Ross Sea since Isotope Stage 3? *7th International Symposium on Antarctic Earth Sciences* **1995**, *10-15 Septemper1995, Siena (Italy), 367*.

59. Anderson, J.B.; Shipp, S.S. Evolution of the West Antarctic Ice Sheet. In: Alley, R., Bindschadler R, . (Eds.), The West Antarctic Ice Sheet: Behavior and Environments, Antarctic Research Series. *American Geophysical Union, Washington, DC,* **2001**, *77*, 45–57.
60. Pico, T.; Mitrovica, J.; Ferrier, K.; Braun, J. Global Ice Volume during MIS 3 Inferred from a Sea-Level Analysis of Sedimentary Core Records in the Yellow River Delta. *Quaternary Science Reviews* **2016**, *152*, doi:10.1016/j.quascirev.2016.09.012.
61. Pasini, G.; Colalongo, M.; Curzi, P.; Taviani, M. Analisi Paleoecologica Degli Ambienti Tardo-Quaternari Del Dosso Gallignani (Adriatico Centro-Meridionale) Mediante Lo Studio Paleontologico Di Carote. *Bollettino della Societa Paleontologica Italiana* **1993**, *32*, 113–130.
62. Jouet, G.; Berne, S.; Rabineau, M.; Bassetti, M.-A.; Bernier, P.; Dennielou, B.; Sierro, F.J.; Flores, J.A.; Taviani, M. Shoreface Migrations at the Shelf Edge and Sea-Level Changes around the Last Glacial Maximum (Gulf of Lions, NW Mediterranean). *Marine Geology* **2006**, *234*, 21–42, doi:10.1016/j.margeo.2006.09.012.
63. Maselli, V.; Trincardi, F.; Asioli, A.; Ceregato, A.; Rizzetto, F.; Taviani, M. Delta Growth and River Valleys: The Influence of Climate and Sea Level Changes on the South Adriatic Shelf (Mediterranean Sea). *Quaternary Science Reviews* **2014**, *99*, 146–163, doi:10.1016/j.quascirev.2014.06.014.
64. Kırcı-Elmas, E.; Nazik, N.; Kapan, S.; Meric, E.; Seker Zor, E.; Kalkan, B.; Dogan, T.; Guney, A. Ponto-Caspian and Mediterranean faunal and floral records of upper Pleistocene-Holocene sediments from the Izmit Gulf (Marmara Sea, Turkey). *Acta Palaeontologica Romaniae* **2021**, *17*, 23–62.
65. Amorosi, A.; Colalongo, M.L.; Fusco, F.; Pasini, G.; Fiorini, F. Glacio-Eustatic Control of Continental–Shallow Marine Cyclicity from Late Quaternary Deposits of the Southeastern Po Plain, Northern Italy. *Quaternary Research* **1999**, *52*, 1–13, doi:10.1006/qres.1999.2049.
66. Amorosi, A.; Colalongo, M.L.; Fiorini, F.; Fusco, F.; Pasini, G.; Vaiani, S.C.; Sarti, G. Palaeogeographic and Palaeoclimatic Evolution of the Po Plain from 150-Ky Core Records. *Global and Planetary Change* **2004**, *40*, 55–78, doi:10.1016/S0921-8181(03)00098-5.
67. Bassetti, M.A.; Berné, S.; Jouet, G.; Taviani, M.; Dennielou, B.; Flores, J.-A.; Gaillot, A.; Gelfort, R.; Lafuerza, S.; Sultan, N. The 100-Ka and Rapid Sea Level Changes Recorded by Prograding Shelf Sand Bodies in the Gulf of Lions (Western Mediterranean Sea). *Geochemistry, Geophysics, Geosystems* **2008**, *9*, doi:10.1029/2007GC001854.
68. Piva, A.; Asioli, A.; Schneider, R.R.; Trincardi, F.; Andersen, N.; Colmenero-Hidalgo, E.; Dennielou, B.; Flores, J.-A.; Vigliotti, L. Climatic Cycles as Expressed in Sediments of the PROMESS1 Borehole PRAD1-2, Central Adriatic, for the Last 370 Ka: 1. Integrated Stratigraphy. *Geochemistry, Geophysics, Geosystems* **2008**, *9*, doi:10.1029/2007GC001713.
69. Maselli, V.; Trincardi, F.; Cattaneo, A.; Ridente, D.; Asioli, A. Subsidence Pattern in the Central Adriatic and Its Influence on Sediment Architecture during the Last 400 Kyr. *Journal of Geophysical Research: Solid Earth* **2010**, *115*, doi:https://doi.org/10.1029/2010JB007687.
70. Kuhlmann, J.; Asioli, A.; Trincardi, F.; Klügel, A.; Huhn, K. Sedimentary Response to Milankovitch-Type Climatic Oscillations and Formation of Sediment Undulations: Evidence from a Shallow-Shelf Setting at Gela Basin on the Sicilian Continental Margin. *Quaternary Science Reviews* **2015**, *108*, 76–94, doi:10.1016/j.quascirev.2014.10.030.
71. Matthews, I.P.; Trincardi, F.; Lowe, J.J.; Bourne, A.J.; MacLeod, A.; Abbott, P.M.; Andersen, N.; Asioli, A.; Blockley, S.P.E.; Lane, C.S.; et al. Developing a Robust Tephrochronological Framework for Late Quaternary Marine Records in the Southern Adriatic Sea: New Data from Core Station SA03-11. *Quaternary Science Reviews* **2015**, *118*, 84–104, doi:10.1016/j.quascirev.2014.10.009.

72. Pellegrini, C.; Asioli, A.; Bohacs, K.M.; Drexler, T.M.; Feldman, H.R.; Sweet, M.L.; Maselli, V.; Rovere, M.; Gamberi, F.; Valle, G.D.; et al. The Late Pleistocene Po River Lowstand Wedge in the Adriatic Sea: Controls on Architecture Variability and Sediment Partitioning. *Marine and Petroleum Geology* **2018**, *96*, 16–50, doi:10.1016/j.marpetgeo.2018.03.002.
73. Campo, B.; Bruno, L.; Amorosi, A. Basin-Scale Stratigraphic Correlation of Late Pleistocene-Holocene (MIS 5e-MIS 1) Strata across the Rapidly Subsiding Po Basin (Northern Italy). *Quaternary Science Reviews* **2020**, *237*, 106300, doi:10.1016/j.quascirev.2020.106300.
74. Antonioli, F.; Ferranti, L. Evidenze Geomorfologiche Sommerse Nelle Aree Costiere Italiane Di Uno Stazionamento Del Livello Del Mare Ubicato a circa – 20 m e Attribuito Allo Stadio 3. *Il Quaternario* **1996**, *9*, 205–208.
75. Taviani, M. The Stage 3 Sea-Level HighsStand and Its Potential Implications on the Decoupling of Antarctic Ice Sheets. *Terra Antartica Reports* **2003**, *8*, 159–161.
76. Doğan, U.; Koçyiğit, A.; Varol, B.; Özer, İ.; Molodkov, A.; Zöhra, E. MIS 5a and MIS 3 Relatively High Sea-Level Stands on the Hatay–Samandağ Coast, Eastern Mediterranean, Turkey. *Quaternary International* **2012**, *Complete*, 65–79, doi:10.1016/j.quaint.2011.12.020.
77. Brunović, D.; Miko, S.; Hasan, O.; Papatheodorou, G.; Ilijanić, N.; Miserocchi, S.; Correggiari, A.; Geraga, M. Late Pleistocene and Holocene Paleoenvironmental Reconstruction of a Drowned Karst Isolation Basin (Lošinj Channel, NE Adriatic Sea). *Palaeogeography, Palaeoclimatology, Palaeoecology* **2020**, *544*, 109587, doi:10.1016/j.palaeo.2020.109587.
78. Surić, M.; Juračić, M.; Horvatinčić, N.; Krajcar Bronić, I. Late Pleistocene–Holocene Sea-Level Rise and the Pattern of Coastal Karst Inundation: Records from Submerged Speleothems along the Eastern Adriatic Coast (Croatia). *Marine Geology* **2005**, *214*, 163–175, doi:10.1016/j.margeo.2004.10.030.
79. Bard, E.; Antonioli, F.; Silenzi, S. Sea-Level during the Penultimate Interglacial Period Based on a Submerged Stalagmite from Argentarola Cave (Italy). *Earth and Planetary Science Letters* **2002**, *196*, 135–146, doi:10.1016/S0012-821X(01)00600-8.
80. Dutton, A.; Bard, E.; Antonioli, F.; Esat, T.M.; Lambeck, K.; McCulloch, M.T. Phasing and Amplitude of Sea-Level and Climate Change during the Penultimate Interglacial. *Nature Geoscience* **2009**, *2*, 355–359, doi:10.1038/ngeo470.
81. Dutton, A.; Scicchitano, G.; Monaco, C.; Desmarchelier, J.M.; Antonioli, F.; Lambeck, K.; Esat, T.M.; Fifield, L.K.; McCulloch, M.T.; Mortimer, G. Uplift Rates Defined by U-Series and 14C Ages of Serpulid-Encrusted Speleothems from Submerged Caves near Siracusa, Sicily (Italy). *Quaternary Geochronology* **2009**, *4*, 2–10, doi:10.1016/j.quageo.2008.06.003.
82. Scicchitano, G.; Monaco, C. Karstic Caves and Submerged Paleo-Shorelines in the Coastal Area between Capo Santa Panagia and Ognina (Siracusa, South-Eastern Sicily). *Alpine and Mediterranean Quaternary* **2006**, *19*, 187–194.
83. Ferranti, L.; Santoro, E.; Mazzella, M.E.; Monaco, C.; Morelli, D. Active Transpression in the Northern Calabria Apennines, Southern Italy. *Tectonophysics* **2009**, *476*, 226–251, doi:10.1016/j.tecto.2008.11.010.
84. Santoro, E.; Mazzella, M.E.; Ferranti, L.; Randisi, A.; Napolitano, E.; Rittner, S.; Radtke, U. Raised Coastal Terraces along the Ionian Sea Coast of Northern Calabria, Italy, Suggest Space and Time Variability of Tectonic Uplift Rates. *Quaternary International* **2009**, *206*, 78–101, doi:10.1016/j.quaint.2008.10.003.
85. Santoro, E.; Ferranti, L.; Burrato, P.; Mazzella, M.E.; Monaco, C. Deformed Pleistocene Marine Terraces along the Ionian Sea Margin of Southern Italy: Unveiling Blind Fault-Related Folds Contribution to Coastal Uplift. *Tectonics* **2013**, *32*, 737–762, doi:10.1002/tect.20036.

86. Zander, A.; Fulling, A.; Brückner, H.; Mastronuzzi, G. OSL Dating of Upper Pleistocene Littoral Sediments: A Contribution to the Chronostratigraphy of Raised Marine Terraces Bordering the Gulf of Taranto, South Italy. *Geografia Fisica e Dinamica Quaternaria* **2006**, *29*, 33–50.
87. Sauer, D.; Wagner, S.; Brückner, H.; Scarciglia, F.; Mastronuzzi, G.; Stahr, K. Soil Development on Marine Terraces near Metaponto (Gulf of Taranto, Southern Italy). *Quaternary International* **2010**, *222*, 48–63, doi:10.1016/j.quaint.2009.09.030.
88. Taviani, M.; Angeletti, L.; Cardone, F.; Montagna, P.; Danovaro, R. A Unique and Threatened Deep Water Coral-Bivalve Biotope New to the Mediterranean Sea Offshore the Naples Megalopolis. *Sci Rep* **2019**, *9*, 3411, doi:10.1038/s41598-019-39655-8.
89. Calcagnile, L.; Maruccio, L.; Scrimieri, L.; delle Side, D.; Braione, E.; D'Elia, M.; Quarta, G. Development and Application of Facilities at the Centre for Applied Physics, Dating and Diagnostics (CEDAD) at the University of Salento during the Last 15 years. *Nuclear Instruments and Methods in Physics Research Section B: Beam Interactions with Materials and Atoms* **2019**, *456*, 252–256, doi:10.1016/j.nimb.2019.03.031.
90. Heaton, T.J.; Köhler, P.; Butzin, M.; Bard, E.; Reimer, R.W.; Austin, W.E.N.; Ramsey, C.B.; Grootes, P.M.; Hughen, K.A.; Kromer, B.; et al. Marine20—The Marine Radiocarbon Age Calibration Curve (0–55,000 Cal BP). *Radiocarbon* **2020**, *62*, 779–820, doi:10.1017/RDC.2020.68.
91. Siani, G.; Paterne, M.; Arnold, M.; Bard, E.; Métivier, B.; Tisnerat, N.; Bassinot, F. Radiocarbon Reservoir Ages in the Mediterranean Sea and Black Sea. *Radiocarbon* **2000**, *42*, 271–280, doi:10.1017/S0033822200059075.
92. Peltier, W.R. Global glacial isostasy and the surface of the ice-age earth: The ICE-5G (VM2) Model and GRACE. *Annual Review of Earth and Planetary Sciences* **2004**, *32*, 111–149, doi:10.1146/annurev.earth.32.082503.144359.
93. Stocchi, P.; Spada, G. Influence of Glacial Isostatic Adjustment upon Current Sea Level Variations in the Mediterranean. *Tectonophysics* **2009**, *474*, 56–68, doi:10.1016/j.tecto.2009.01.003.
94. Lisiecki, L.E.; Raymo, M.E. A Pliocene-Pleistocene Stack of 57 Globally Distributed Benthic Δ18O Records. *Paleoceanography* **2005**, *20*, doi:https://doi.org/10.1029/2004PA001071.
95. Argus, D.F.; Peltier, W.R.; Drummond, R.; Moore, A.W. The Antarctica Component of Postglacial Rebound Model ICE-6G_C (VM5a) Based on GPS Positioning, Exposure Age Dating of Ice Thicknesses, and Relative Sea Level Histories. *Geophysical Journal International* **2014**, *198*, 537–563, doi:10.1093/gji/ggu140.
96. de Boer, B.; Stocchi, P.; Whitehouse, P.L.; van de Wal, R.S.W. Current State and Future Perspectives on Coupled Ice-Sheet – Sea-Level Modelling. *Quaternary Science Reviews* **2017**, *169*, 13–28, doi:10.1016/j.quascirev.2017.05.013.
97. de Boer, B.; Stocchi, P.; van de Wal, R.S.W. A Fully Coupled 3-D Ice-Sheet–Sea-Level Model: Algorithm and Applications. *Geoscientific Model Development* **2014**, *7*, 2141–2156, doi:10.5194/gmd-7-2141-2014.
98. Gowan, E.J.; Zhang, X.; Khosravi, S.; Rovere, A.; Stocchi, P.; Hughes, A.L.C.; Gyllencreutz, R.; Mangerud, J.; Svendsen, J.-I.; Lohmann, G. A New Global Ice Sheet Reconstruction for the Past 80 000 Years. *Nature Communications* **2021**, *12*, 1199, doi:10.1038/s41467-021-21469-w.
99. Antonioli, F.; Furlani, S.; Montagna, P.; Stocchi, P.; Calcagnile, L.; Quarta, G.; Cecchinel, J.; Presti, V.L.; Morticelli, M.G.; Martin, F.F.; et al. Submerged Speleothems and Sea Level Reconstructions: A Global Overview and New Results from the Mediterranean Sea. *Water* **2021**, *13*, 1663, doi:10.3390/w13121663.
100. Antonioli, F.; Ferranti, L.; Stocchi, P.; Deiana, G.; Lo Presti, V.; Furlani, S.; Marino, C.; Orru, P.; Scicchitano, G.; Trainito, E.; et al. Morphometry and Elevation of the Last Interglacial Tidal Notches in Tectonically Stable Coasts of the Mediterranean Sea. *Earth-Science Reviews* **2018**, *185*, 600–623, doi:10.1016/j.earscirev.2018.06.017.
101. Pico, T.; Creveling, J.R.; Mitrovica, J.X. Sea-Level Records from the U.S. Mid-Atlantic Constrain Laurentide Ice Sheet Extent during Marine Isotope Stage 3. *Nat Commun* **2017**, *8*, 15612, doi:10.1038/ncomms15612.